Journal of Materials Chemistry A

COMMUNICATION

View Article Online
View Journal | View Issue

Cite this: J. Mater. Chem. A, 2018, 6, 24676

Received 30th September 2018
Accepted 26th October 2018

DOI: 10.1039/c8ta09486a

rsc.li/materials-a

Highly efficient uranium adsorption by salicylaldoxime/polydopamine graphene oxide nanocomposites†

Yongxin Qian,[a] Yihui Yuan,[a] Heliang Wang,[a] Hu Liu,[bc] Jiaoxia Zhang,[bd] Se Shi,*[a] Zhanhu Guo*[b] and Ning Wang*[a]

Uranium is the main element for nuclear energy production and is one of the most hazardous radionuclides; its effective enrichment plays a key role in energy strategy and environmental safety. Oxime-functionalized nanostructures are the most promising candidates for uranium adsorption. However, current methods for their preparation mainly focus on multistep grafting and oximation processes, and the nanostructures usually show low efficiency. Here, we report a rapid one-step process to synthesize salicylaldoxime/polydopamine modified reduced graphene oxide (RGO-PDA/oxime) *via* the polymerization of dopamine (DA) and simultaneous deposition of oxime with an obviously decreased total synthesis time of 2 h. The obtained maximum uranium adsorption capacity of up to 1049 mg g^{-1} was 3–16 times larger than those of the reported single PDA or oxime modified nanostructures. The RGO-PDA/oxime followed the pseudo-second-order kinetics model and Langmuir isotherm equation with much higher adsorption selectivity and recyclability. The outstanding sorption performance is attributed to the electrostatic repulsion between GO and salicylaldoxime and the effective combination between PDA and oxime molecules. Finally, given the adhesion capability of DA to diverse surfaces, this rapid one-step method was used to prepare five other oxime/PDA modified materials, which also showed improved uranium adsorption efficiency. These findings provide a way to obtain oxime-functionalized nanostructures with promising uranium adsorption efficiency.

1 Introduction

Nuclear power is well known as a clean and highly efficient energy source and is regarded as a key component of energy systems.[1] Uranium, as a strategic source of nuclear power, has attracted extensive attention. However, uranium-containing wastes, discharged from the nuclear fuel cycle or nuclear accidents, have radioactivity and chemical toxicity.[2] Meanwhile, vast uranium reserves are necessary for energy security and the reduction of greenhouse gas emission. Therefore, it is vital to develop efficient techniques to remove and recover uranium from nuclear waste solutions or other solutions for environmental safety and creation of nuclear energy reserves. Various techniques, including adsorption,[3] membrane filtration,[4] chemical precipitation,[5] ion exchange,[6] and solvent extraction[7] were used to enrich uranium or other heavy metals. Among them, adsorption is a very popular approach to remove heavy metals and other pollutants due to its high efficiency, convenient operation, low cost, *etc.*[8,9] Combining the structure character of nanomaterials and the coordination capability of functional molecules to synthesize functionalized nanostructure materials for uranium adsorption has attracted increasing attention.[10–12] Among nanomaterials, the nanostructures with larger surface area, low weight, dense binding sites and rapid mass transfer are usually applied as the adsorption substrates.[13,14] For functional molecules, amidoxime and oxime are verified to be the most promising groups for uranium adsorption owing to their high coordination affinity and selectivity towards the uranyl ion.[15,16]

The immobilization of oxime-containing molecules on nanostructure surfaces plays a key role in uranium adsorption. A more effective immobilized oxime group normally has a higher uranium adsorption capability. Connecting nitrile onto the nanostructures through amino–carboxyl reactions, siloxane coupling reactions, radiation-induced graft polymerization (RIGP) and atom-transfer radical polymerization (ATRP), and then converting the nitrile into an oxime product *via* treatment with hydroxylamine, is the most common approach to prepare

[a]State Key Laboratory of Marine Resource Utilization in South China Sea, Hainan University, Haikou 570228, China. E-mail: wangn02@foxmail.com; shise@hainu.edu.cn

[b]Integrated Composites Laboratory (ICL), Department of Chemical & Biomolecular Engineering, University of Tennessee, Knoxville, TN 37996, USA. E-mail: zguo10@utk.edu

[c]Key Laboratory of Materials Processing and Mold, Ministry of Education, National Engineering Research Center for Advanced Polymer Processing Technology, Zhengzhou University, Zhengzhou 450002, China

[d]School of Materials Science and Engineering, Jiangsu University of Science and Technology, Zhenjiang, Jiangsu 212003, China

† Electronic supplementary information (ESI) available. See DOI: 10.1039/c8ta09486a

oxime-containing materials.[17–20] However, two major defects exist in these methods. On one hand, the multi-step process and difficult graft reactions result in inferior immobilization efficiency of the nitrile. On the other hand, treatment with hydroxylamine is demanding, time-consuming (even needs many days) and complicated.[21,22] It is crucial to develop convenient and rapid methods to prepare oxime-functionalized nanostructured materials for highly efficient uranium adsorption.

Dopamine (DA) can adhere to the surfaces of almost all substrates *via* self-polymerization.[23] The polymerization is very rapid; specifically, 10 min is sufficient for the substrates to achieve a relatively successful polydopamine (PDA) functional layer.[24] Although the polymerization mechanism is unclear, plentiful functional groups (such as amino and imino groups, indole units, and catechol and quinone functions) and strong noncovalent interactions (including electrostatic interactions, hydrogen bonding, π–π stacking, coordination or chelation, and charge transfer) exist in PDA. These groups and interactions supply PDA with superior adhesion and secondary reaction activities.[25–30] Due to the versatility of PDA, it has been applied to uranium adsorption *via* simple polymerization of DA on different substrate surfaces (including mesoporous silica nanospheres, mesoporous molecular sieves, magnetic nanoparticles, and glass fiber carpets) based on the chelation and coordination of the catechol and amino in PDA to uranium(VI).[2,31,32] However, their adsorption capabilities were very low; the main reason for the inferior adsorption behavior may be that PDA is suitable for surface modification rather than for adsorption.

The aims of this project are to address the time-consumption, complexity, and inferior oximation efficiency of the current methods for the preparation of oxime-functionalized nanostructured materials and to combine the versatile surface modification property of PDA with the excellent coordination ability of oxime groups to uranyl ions. Herein, we report a one-step process for the convenient and rapid synthesis of oxime/PDA modified reduced graphene oxide (RGO-PDA/oxime) composites with highly efficient uranium adsorption capability. The schematic illustration is shown in Fig. 1. Compared with the reported methods, at least two breakthroughs were reached in this work. On one hand, unlike the multistep grafting and oximation reactions, this process was realized *via* a simple one-step mixing of DA, oxime and GO. The fabrication time decreased to 2 h, which was only 1–19% of those of the reported oxime-functionalized nanostructures. On the other hand, instead of the traditional surface modification reagents, PDA was used as a functional material to immobilize salicylaldoxime as much as possible on the sample surface *via* electrostatic interaction, hydrogen bonding and π–π stacking. Meanwhile, oxime preferred to distribute on the upper surface of the samples due to the electrostatic repulsion between GO and salicylaldoxime. These two features endowed the RGO-PDA/oxime with excellent properties with a maximum uranium adsorption amount of 1049 mg g^{-1}. Furthermore, the prepared adsorbent was still stable after four cycles of uranium adsorption–desorption; the sorption process was in good agreement with the second-order kinetics equation and Langmuir model. Finally, other substrates were studied to explore their potential application in the preparation of oxime-functionalized nanostructure materials for highly efficient uranium adsorption.

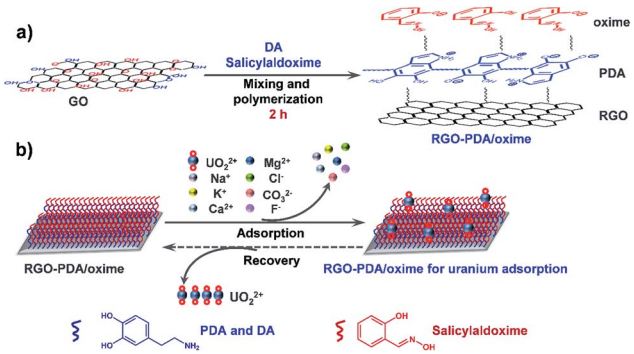

Fig. 1 Schematic illustration of the synthesis of the RGO-PDA/oxime (a) and the adsorption of uranium by the prepared RGO-PDA/oxime (b). The RGO-PDA/oxime was formed by a one-step process *via* simple mixing of GO, DA and salicylaldoxime. Oxime preferred to be distributed on the upper surface of the samples due to the electrostatic repulsion between GO and salicylaldoxime. The prepared samples exhibited excellent adsorption capability to uranyl ions and can be recycled over four times.

2 Experimental

2.1 Synthesis of RGO-PDA and RGO-PDA/oxime composites

RGO-PDA/oxime. 40 mg GO (prepared *via* the typically modified Hummers' method) was dispersed in 20 mL tris(hydroxymethyl)aminomethane (Tris) buffer (10 mM). Then, 40 mg DA (purchased from Sigma-Aldrich) and 80 mg salicylaldoxime (purchased from Energy Chemical Co., Ltd.) were added to the GO dispersion at the same time. After adjusting the pH to 8.5, the mixture was stirred vigorously for 2 h at room temperature. The product was centrifuged, repeatedly washed with deionized water, and lyophilized overnight. Finally, the oxime/PDA-functionalized GO was obtained.

RGO-PDA. As a comparative experiment, the RGO-PDA was prepared *via* the same method as that of RGO-PDA/oxime, except that salicylaldoxime was not added in the reaction.

2.2 Characterization

Zeta potential values were measured using a Zetasizer Nano S90 (Malvern Instruments Ltd.). The microstructures and energy dispersive spectrometry (EDS) images were observed using a Hitachi S-4800 scanning electron microscope (SEM) and on a Bruker Multimode 8 system. Fourier transform infrared (FT-IR) data were obtained using a PerkinElmer FT-IR spectrometer under normal conditions. UV-vis spectra and the concentration of uranium were measured using an UV1800PC UV-visible spectrophotometer. X-ray photoelectron spectroscopy (XPS) data were measured on a Kratos Axis Supra spectrophotometer. Thermogravimetric analysis (TGA) was

performed by using a TA Instruments SDT-Q600 system. Nitrogen adsorption–desorption isotherms were obtained on a Micromeritics ASAP 2460 instrument, and the specific surface area and intra porosity data were determined by the Brunauer–Emmett–Teller (BET) and Barrett–Joyner–Halenda (BJH) methods, respectively.

2.3 Adsorption experiments

For the adsorption experiment, uranium solutions of 8, 16, 32, 50, 80 and 100 mg L^{-1} were prepared by dissolving $UO_2(NO_3)_2 \cdot 6H_2O$ in deionized water, respectively. Then, 5 mg GO, RGO-PDA and RGO-PDA/oxime composites were added to the prepared uranium solutions (500 mL), respectively, and the mixtures were placed in a shaker at 300 rpm at room temperature. After the adsorption process, the samples were separated by centrifugation, and the uranium concentration in the supernatant was measured by spectrometry based on the chromogenic reaction between arsenazo-III and U(VI). At this stage, the pH of the uranium solutions was adjusted by adding 0.3 M NaOH and HNO_3. The adsorption capacity for uranium was calculated according to eqn (1).

$$q_e = (C_o - C_e)V/m \quad (1)$$

where q_e (mg g^{-1}) represents the sorption amount of the adsorbent, C_o (mg L^{-1}) and C_e (mg L^{-1}) are the uranium concentrations at the initial and equilibrium states, respectively, V (L) is the solution volume and m (g) is the adsorbent weight.

2.4 Adsorption tests in simulated seawater

Simulated seawater was prepared by dissolving 33 g sea salt in 1 L deionized water. In the adsorption experiment, 5 mg RGO-PDA/oxime was added to 500 mL simulated seawater and stirred at 300 rpm at room temperature. After the adsorption process, the adsorbents were separated using a centrifuge. Finally, the uranium content in the supernatant was analyzed by spectrometry.

2.5 Elution of uranium and regeneration of the RGO-PDA/oxime adsorbent

The uranium-loaded RGO-PDA/oxime (10 mg) was immersed in 50 mL eluant (1 M Na_2CO_3 and 0.1 M H_2O_2) at room temperature and stirred for 30 min. Equal amounts of eluent were collected after 2.5, 5, 7.5, 10, 15, 20, 25, and 30 min, respectively, and then the uranium concentration in the eluent was analysed by the arsenazo-III spectrophotometric method.

After elution, the RGO-PDA/oxime was collected by centrifugation, washed with deionized water, lyophilized overnight, and then used for the next adsorption experiment *via* the same method as described above. The adsorption capability of the recycled adsorbents was determined by the same arsenazo spectrophotometric strategy. The recyclability of the RGO-PDA/oxime was evaluated by these continuous adsorption–desorption cycle experiments.

2.6 Oxime/PDA functionalization and adsorption experiments for other nanostructured substrates

In this section, five nanostructured materials, including graphite, Fe_2O_3 nanoparticles (NPs), polystyrene spheres (PS), carbon nanotubes (CNTs) and metal–organic frameworks (MOFs) were used as the model substrates. The synthesis and adsorption experiments of the oxime/PDA modified substrates were performed *via* the same method as those for the RGO-PDA/oxime, respectively. Meanwhile, as a comparison, the uranium adsorption amounts were determined for these bare (before oxime modification) substrates, and the results were compared with the data of the oxime/PDA-modified substrates.

3 Results and discussion

3.1 Synthesis and characterization of RGO-PDA/oxime

RGO-PDA/oxime was produced *via* a simple one-step process by mixing GO with DA and salicylaldoxime in Tris buffer. After shaking for 2 hours at room temperature, the brown yellow GO suspension turned into a dark black solution. During this stage, DA was polymerized onto GO and the oxime was deposited on the sample surface simultaneously. Meanwhile, GO was reduced to reduced GO (RGO) due to the oxidative polymerization of DA.[33] In addition, oxime was exposed on the surface of the RGO-PDA/oxime owing to the electrostatic repulsion between the negatively charged GO and salicylaldoxime. The UV-vis spectrum of the RGO-PDA/oxime solution demonstrated that PDA and oxime remained stable. A new peak at 281 nm (the characteristic absorption of PDA owing to the presence of catechol[34]) was detected for RGO-PDA. The peaks at 257 nm and 304 nm (the characteristic absorption of salicylaldoxime) were present for the RGO-PDA/oxime (Fig. 2a). The surface functionalization of the prepared samples was further characterized by FT-IR spectroscopy. As shown in Fig. 2b, a feature at 1510 cm^{-1} (assigned to the N–H bending vibration) was detected in the RGO-PDA and RGO-PDA/oxime, indicating the presence of PDA in the formed products. Compared with RGO-PDA, an additional peak at 1610 cm^{-1} (assigned to the C=N stretching vibration) was detected in the RGO-PDA/oxime, demonstrating the presence of the oxime groups in the prepared GO-PDA/oxime. In addition, the decrease of the peak at 1727 cm^{-1} was an indication of the reduction of GO for the RGO-PDA and RGO-PDA/oxime.

The surface morphology and thickness of the synthesized RGO-PDA/oxime were evaluated by the SEM and AFM techniques. As shown in Fig. 3a, the twisted RGO sheets were cross-linked randomly, forming a porous 3D structure. The self-assembly of GO sheets can result from the partial overlapping and coalescence of flexible RGO through noncovalent interactions (such as hydrogen bonding and π–π interactions).[35] The high-magnification SEM image (Fig. 3b) showed hardly any large PDA particles (resulting from the self-polymerization of DA) on the GO surface due to the high affinity between the PDA aromatic rings and GO. AFM analysis (Fig. 3c) showed that the samples had a relatively smooth surface, which further demonstrated that DA and oxime were deposited uniformly on

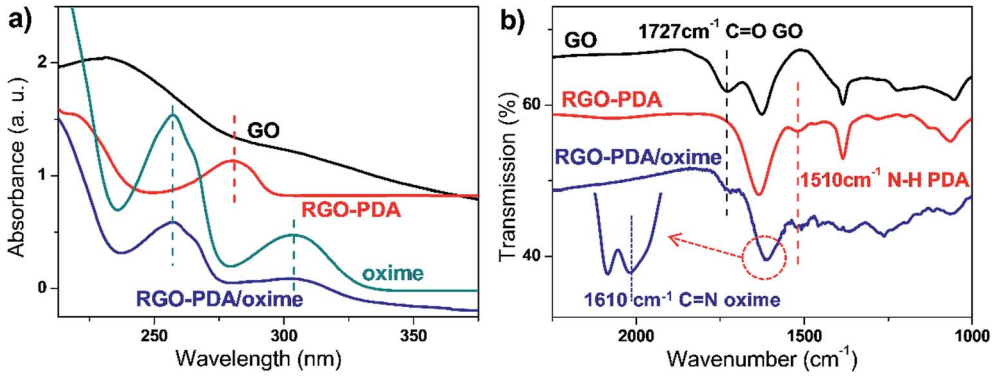

Fig. 2 UV-vis (a) and FT-IR (b) spectra of GO, RGO-PDA and RGO-PDA/oxime.

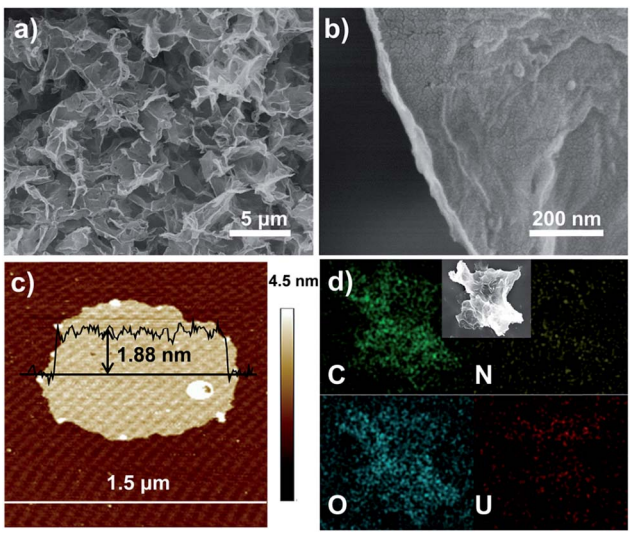

Fig. 3 SEM (a), high-magnification SEM (b) and AFM (c) images showing the cross-linking, microstructure, and thickness of the prepared RGO-PDA/oxime, respectively. The EDS mapping (d) image showing the elemental distribution of the prepared RGO-PDA/oxime after uranium adsorption for 12 h with an initial uranium concentration of 32 mg L^{-1}.

the GO surface. Moreover, after the deposition, the samples still maintained a thin layer with an average thickness of 1.88 nm (in contrast, the average thickness of GO was 0.93 nm, as shown in Fig. S1a, ESI†).

The static water contact angle of the RGO-PDA/oxime was 28.91° (as shown in Fig. S2, ESI†), this excellent hydrophilicity indicated a perfect adsorption capacity of the adsorbents. TGA was performed to quantify the PDA/oxime content in the RGO-PDA/oxime composites. The content of PDA/oxime in the RGO-PDA/oxime composites was determined by the weight loss at 200 °C to 400 °C, which was about 20 wt% (Fig. S3, ESI†). The BET and BJH results indicated that the surface area and pore volume of the RGO-PDA/oxime composites were 127.28 cm^2 g^{-1} and 0.56 cm^3 g^{-1} (Fig. S4, ESI†), respectively, which could promote the adsorption of uranium. The elemental distribution of the RGO-PDA/oxime after the adsorption of uranium was estimated by EDS mapping. Fig. 3d shows that a significant amount and homogeneous distribution of the captured uranium was present on the samples.

3.2 Effects of pH on uranium adsorption

pH has a remarkable influence on uranium adsorption since it affects the speciation distribution of uranium in solution and the surface charges of the binding sites of the adsorbent. The effects of pH on uranium adsorption by RGO-PDA/oxime were investigated in an initial pH range of 3–8. The results indicated that pH had a strong influence on uranium adsorption on the RGO-PDA/oxime surface. As shown in Fig. 4a (red line), the adsorption capacities of the samples increased dramatically at pH 3–5, then remained relatively constant at pH 5–6, and finally decreased with a further increase in pH. The optimal pH value was 5 for uranium adsorption on the RGO-PDA/oxime surface.

The species distribution of uranium and surface charges of the samples affect the interaction between uranium(VI) and RGO-PDA/oxime, which results in diverse adsorption behaviors at different pH values. At pH ≤ 5, uranium(VI) existed in the solution with the positively charged species. As the pH increased, the electrostatic interactions between these cations and RGO-PDA/oxime increased due to the enhancement of the deprotonation of salicylaldoxime and PDA (the zeta potential values of RGO-PDA/oxime in different pH solutions are shown by the blue line of Fig. 4a), thereby strengthening the adsorption capability. When the pH > 5, the neutrally charged uranium(VI) species increased (the negatively charged uranium(VI) species even became the dominating form when the pH > 8);[31] the electrostatic repulsion increased between these anions and highly negatively charged RGO-PDA/oxime, thus weakening the adsorption capability.

3.3 Sorption kinetics

Sorption rate is a key parameter used to estimate the performance of the absorbent. In order to evaluate the sorption kinetics, the influence of the contact time on uranium adsorption on the RGO-PDA/oxime surface was performed with an initial uranium concentration of 8 mg L^{-1}. As shown in Fig. 4b (blue line), the sorption capacity of the RGO-PDA/oxime exhibited a significant increase at first, then increased slowly,

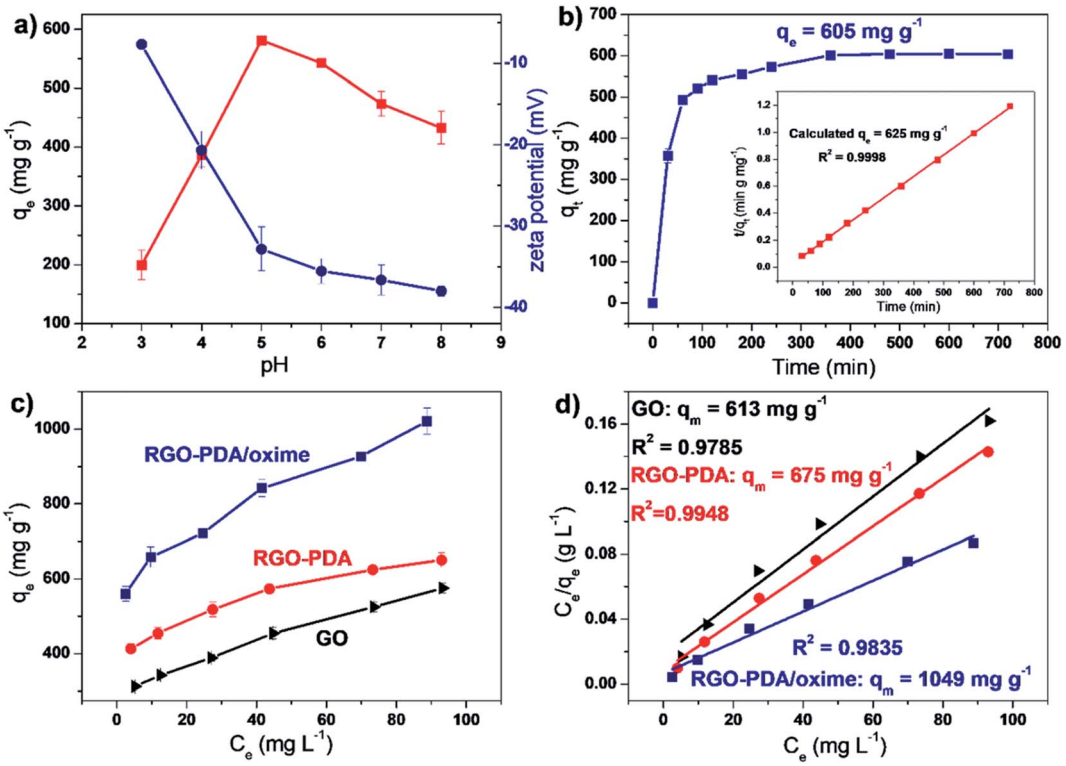

Fig. 4 Effects of pH on uranium adsorption ((a) red line) and zeta potential values of the RGO-PDA/oxime in different pH solutions ((a) blue line). C_o = 8 mg L^{-1}, t = 6 h and T = 298 K. Kinetics ((b) blue line) and pseudo-second-order kinetics model ((b) inset) of uranium adsorption on the RGO-PDA/oxime surface. C_o = 8 mg L^{-1}, pH = 5.0 ± 0.1 and T = 298 K. Sorption isotherms of uranium (c) and plots of the Langmuir adsorption model (d) for RGO-PDA/oxime, RGO-PDA and GO, respectively. pH = 5.0 ± 0.1, t = 6 h and T = 298 K.

and remained virtually unchanged after a contact time of 6 h, demonstrating that the adsorption of uranium(VI) on the RGO-PDA/oxime was accomplished. The maximum adsorption capability of uranium was 605 mg g^{-1} (C_o = 8 mg L^{-1}) when the adsorption achieved an equilibrium at a contact time of 6 h.

To further evaluate the adsorption behaviors of the samples, pseudo-first-order and pseudo-second-order kinetics models (as shown in eqn (2) and (3), respectively[36]) were applied to analyze the dynamic processes.

$$\ln(q_e - q_t) = \ln q_e - k_1 t \quad (2)$$

$$\frac{t}{q_t} = \frac{1}{k_2 q_e^2} + \frac{t}{q_e} \quad (3)$$

where q_e (mg g^{-1}) and q_t (mg g^{-1}) represent the adsorption capabilities at equilibrium and a certain time, respectively. k_1 (min^{-1}) and k_2 (g (mg min)$^{-1}$) are the rate constants of the corresponding kinetics models, respectively. The values of q_e, k_1 and k_2 were calculated according to the slopes and intercepts of the plots (red line of the inset in Fig. 4b and S7, ESI†), which are shown in Table S1 (ESI).† The coefficient of determination (R^2) of the second-order kinetics equation was 0.9998, which was higher than that (0.9085) of the first-order kinetics equation. In addition, the value of the calculated equilibrium adsorption amount for the second-order kinetics equation was 625 mg g^{-1}, which was closer to the obtained experimental result (q_e = 605 mg g^{-1}) than that (257 mg g^{-1}) of the first-order adsorption kinetics equation. These results indicated that the pseudo-second-order kinetics expression was more appropriate for the adsorption mechanism and the adsorption of uranium(VI) on the RGO-PDA/oxime surface was a chemisorption process.

3.4 Sorption isotherms

Coordination of =N–O– groups with UO_2^{2+} endows the oxime-modified materials with adsorption capability to uranium(VI). The more effective the oxime group immobilization is, the more uranium will be adsorbed. This work combined the excellent adhesion ability of PDA with the outstanding coordination capability of oxime groups to uranium(VI) and developed a rapid one-step method to synthesize oxime-functionalized nanostructured materials, *i.e.* RGO-PDA/oxime. To evaluate its maximum sorption capacity, the sorption isotherm of the RGO-PDA/oxime was determined by increasing the initial concentration of uranyl ions from 8 mg L^{-1} to 100 mg L^{-1} at pH 5 and 298 K. The comparative experiments were done by measuring the equilibrium adsorption amounts for RGO-PDA and GO, respectively, at the same initial uranium(VI) concentrations as those for the RGO-PDA/oxime. As shown in Fig. 4c, the adsorption capacity of these three samples increased in the uranyl ion concentration at adsorption equilibrium. Furthermore, it is apparent that the adsorption capacity of the RGO-PDA/oxime was much larger than those of RGO-PDA and GO.

The experimental values of the maximum sorption capacities of RGO-PDA/oxime, RGO-PDA and GO were 1021 mg g^{-1}, 650 mg g^{-1} and 575 mg g^{-1}, respectively.

To further investigate the adsorption behavior of the samples, the Langmuir and Freundlich equations were applied to describe the adsorption isotherms. Generally speaking, the Langmuir model hypothesizes that all binding sites possess the same adsorption intensity and the adsorption is localized in a monolayer; the Freundlich equation supposes that the adsorption takes place on the heterogeneous surfaces. The two models are expressed by eqn (4) and (5), respectively.[37]

$$\frac{C_e}{q_e} = \frac{1}{q_m K_L} + \frac{1}{q_m} C_e \quad (4)$$

$$\log q_e = \log K_F + n \log C_e \quad (5)$$

where C_e (mg L^{-1}) represents the uranyl ion concentration at equilibrium. q_e (mg g^{-1}) and q_m are the equilibrium sorption capability and maximum sorption amount, respectively. K_L, K_F and n are the Langmuir and Freundlich parameters related to the adsorption energy, adsorption capacity and the adsorption intensity, respectively. The values of q_m, K_L, K_F and n were calculated according to the intercepts and slopes of the plots (Fig. 4d and S8, ESI†), which are listed in Table S2 (ESI).† The results demonstrated that the isotherms fit closer to the Langmuir model ($R_{RGO\text{-}PDA/oxime}^2 = 0.9835$, $R_{RGO\text{-}PDA}^2 = 0.9948$ and $R_{GO}^2 = 0.9785$) than to the Freundlich model ($R_{RGO\text{-}PDA/oxime}^2 = 0.9420$, $R_{RGO\text{-}PDA}^2 = 0.9736$ and $R_{GO}^2 = 0.9388$), which demonstrated that the adsorption of uranium(VI) on these three sample surfaces occurred at homogeneous binding sites and a monolayer was formed. In addition, according to the Langmuir adsorption expression, the calculated maximum sorption amount (1049 mg g^{-1}) for RGO-PDA/oxime was much larger than those (675 mg g^{-1} and 613 mg g^{-1}, respectively) for RGO-PDA and GO, and these results were close to the corresponding experimental data. Furthermore, the maximum adsorption capacity of the RGO-PDA/oxime was 3.16–16.09 times larger than those of the reported single PDA or oxime modified nanostructured materials for uranium(VI) adsorption, and the fabrication time of the RGO-PDA/oxime was only 1–19% of those of the reported oxime-functionalized uranium adsorption materials (Table 1).[19,31,32,38–40] In addition, the uranium adsorption capability of this reported RGO-PDA/oxime was much higher than those (47 mg g^{-1} for RGO, 134 mg g^{-1} for RGO hydrogel, and 278 mg g^{-1} for layered double hydroxide/RGO) of other reported RGO-based adsorbents.[41–43] These results indicate that the immobilization of oxime on the nanostructure surface *via* the interfacial polymerization of DA is a rapid method to synthesize uranium adsorption materials, and the synthesized samples exhibit highly efficient uranium adsorption capability.

There are some reasons for the high uranium adsorption efficiency of the prepared RGO-PDA/oxime. Firstly, the large specific surface area of GO promotes the adsorption ability of GO-based materials. Secondly, the excellent surface modification of PDA caused more oxime molecules to be immobilized onto the surface of the samples. Furthermore, oxime was considered to be the most promising functional group for the chelation of uranium owing to its high affinity to uranyl ions. Previous studies have confirmed that =N–OH groups can be deprotonated and then chelate UO_2^{2+}.[44,45] In this work, we proved that =N–OH groups successfully conjugated with UO_2^{2+} by XPS spectroscopy. XPS measurement was performed in order to investigate the chemical composition before and after uranium adsorption. In contrast to the survey spectrum of RGO-PDA/oxime, a new strong U 4f peak can be observed unambiguously in the spectrum of RGO-PDA/oxime-U (Fig. 5b). As shown in the corresponding high resolution spectrum of the peaks around U 4f, the binding energy regions at 392.20 eV and 381.72 eV are the U $4f_{5/2}$ and U $4f_{7/2}$ (Fig. 5c),[46] respectively, which indicated the presence of uranium in RGO-PDA/oxime-U. In addition, the O 1s spectrum of RGO-PDA/oxime before uranium adsorption can be fitted to two peaks, which are attributed to C–O and N–O (in the =N–OH groups), respectively. After uranium adsorption, a new peak centered at 531.55 eV, which can be ascribed to the O=U=O group, indicates the loading of uranium on the RGO-PDA/oxime surface. Moreover, the position of N–O was shifted to a lower binding energy from 532.60 eV to 532.30 eV (Fig. 5d), which could be attributed to the chelation of UO_2^{2+} with the oxime groups of the RGO-PDA/oxime.

Table 1 Comparison of the maximum adsorption amount (of uranium) and fabrication time of the prepared RGO-PDA/oxime with those of other reported single PDA or oxime functionalized sorbents

Samples	q_m[a] (mg g^{-1})	Fabrication time (h)	References
$mSiO_2$/PDA	332.3	24	31
SBA-15/PDA	196	3	32
Oxime-CMK-5	65.18	10.5	38
Fe_3O_4@SiO_2–AO	104.96	34	19
AO-*g*-MWCNTs	176	16	39
PAF-1-CH_2AO	304	192	40
RGO-PDA/oxime	**1049**	**2**	**This work**

[a] q_m: maximum adsorption amount calculated from the Langmuir isotherm model.

3.5 Effects of co-existing ions and the simulated seawater testing

To evaluate the adsorption selectivity of the RGO-PDA/oxime, adsorption experiments were performed in simulated seawater at pH 5 and initial uranium concentrations of 8 mg L^{-1}, 16 mg L^{-1} and 32 mg L^{-1}, respectively. The simulated seawater was prepared by dissolving 33 g sea salt in 1 L deionized water, *i.e.* K^+, Na^+, Mg^{2+}, Ca^{2+}, Sr^{2+}, Cl^-, Br^-, SO_4^{2-}, HCO_3^-, CO_3^{2-} and F^- co-existed in the test solution and their concentrations were thousand times higher than that of uranium. As shown in Fig. 5e, the adsorption amounts of uranium in the simulated seawater were 503.16 mg g^{-1} (C_o = 8 mg L^{-1}), 627.76 mg g^{-1} (C_o = 16 mg L^{-1}) and 721.24 mg g^{-1} (C_o = 32 mg L^{-1}), respectively, and these data were close to those (549.48 mg g^{-1}, 658.25 mg

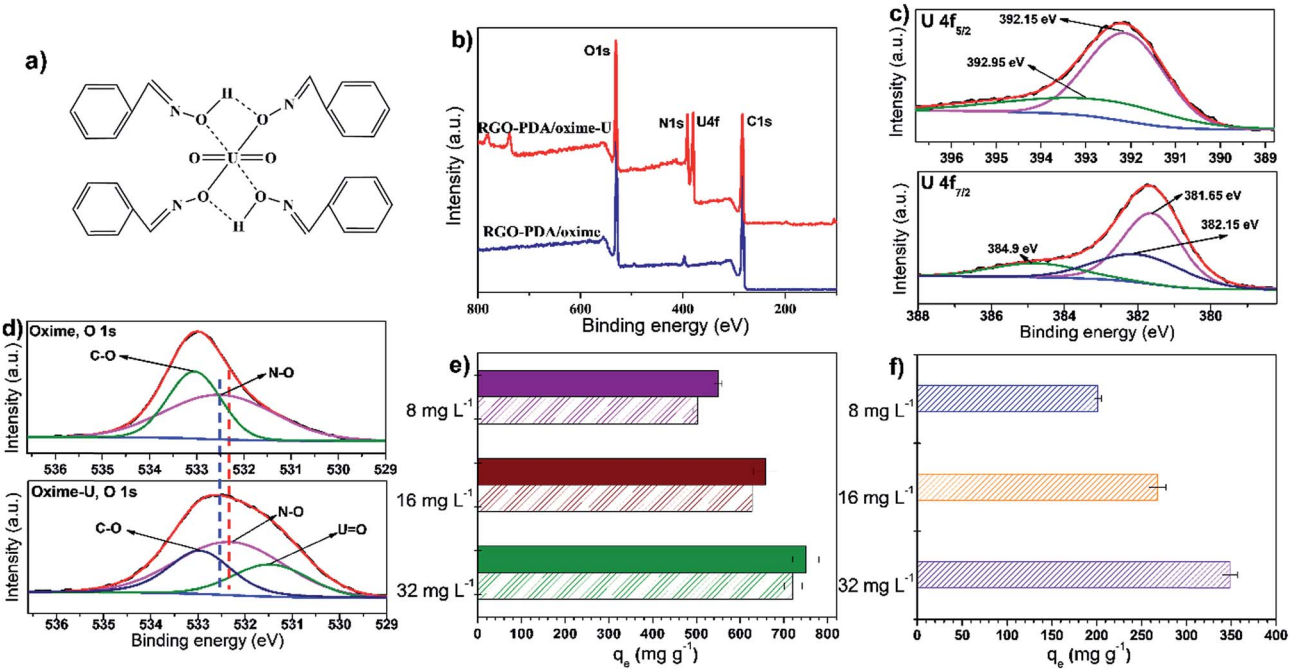

Fig. 5 (a) The bonding mechanism between UO_2^{2+} and the oxime group of RGO-PDA/oxime. (b) The XPS spectra before and after uranium loading on the RGO-PDA/oxime. (c) High resolution XPS spectra of U 4f of RGO-PDA/oxime-U. (d) High resolution XPS spectra of O 1s of RGO-PDA/oxime and RGO-PDA/oxime-U, respectively. (e) Adsorption selectivity by measuring the sorption capacities for uranium(VI) at different initial uranium(VI) concentrations (8 mg L^{-1}, 16 mg L^{-1} and 32 mg L^{-1}, respectively) in aqueous solution (solid bars) and simulated seawater (hatched bars). pH = 5.0 ± 0.1, t = 6 h and T = 298 K. (f) Adsorption capability of the RGO-PDA/oxime in simulated seawater for uranium(VI) with different initial uranium(VI) concentrations (8 mg L^{-1}, 16 mg L^{-1} and 32 mg L^{-1}, respectively). pH = 8.0 ± 0.1, t = 6 h and T = 298 K.

g^{-1} and 750.35 mg g^{-1} at the corresponding initial uranium concentration, respectively) in the aqueous solution. These results indicated that the RGO-PDA/oxime possessed an excellent binding capability for the selective separation of uranium(VI) in complex aqueous solutions.

Based on the high adsorption capacity and adsorption selectivity of the RGO-PDA/oxime in aqueous solutions, its adsorption capacity was investigated under simulated seawater conditions. The simulated seawater was prepared by dissolving 33 g sea salt in 1 L deionized water. The results (Fig. 5f) showed that the adsorption amounts of uranium in simulated seawater (pH = 8.0) were 201.62, 267.70 and 348.62 mg g^{-1} for the initial uranium concentrations of 8, 16 and 32 mg L^{-1}, respectively, further demonstrating that the RGO-PDA/oxime composites can be used for uranium removal and uranium enrichment in real seawater.

3.6 Elution of uranium and regeneration of the RGO-PDA/oxime adsorbent

For practical applications, an excellent adsorbent should have not only high adsorption capacity but also good reutilization ability to reduce its overall cost. In this work, 1 M Na_2CO_3 containing 0.1 M H_2O_2 was used as the eluant, and the uranium concentration in the eluent was measured to evaluate the elution efficiency. As shown in Fig. S9a (ESI),† ~73% of uranium was released from the RGO-PDA/oxime within 10 min, and the elution efficiency reached ~97% when the elution was continued for 30 min. In contrast, when deionized water was used as the eluent, only 3% of uranium could be released from the adsorbent. The high efficiency elution may be attributed to the formation of an extremely stable uranyl-peroxo-carbonato complex.[47] The regeneration ability of the prepared adsorbents was estimated by the continuous adsorption–desorption cycle experiments. Fig. S9b (ESI)† shows that the adsorption efficiency of the RGO-PDA/oxime remained at least 90% after it was recycled four times. This high regeneration efficiency of RGO-PDA/oxime composites indicates their potential application in extracting U(VI) from solutions.

3.7 Immobilization of oxime on other nanostructured substrates and their adsorption capabilities

Considering that PDA can adhere to various surfaces, the immobilization of the oxime onto other nanostructures *via* this reported one-step process and whether these fabricated oxime-functionalized materials possessed a progressive uranium adsorption property were tested. Five different substrates, including graphite, Fe_2O_3 NPs, PS, CNTs and MOFs, were chosen as the model substrates. Salicylaldoxime was immobilized onto these surfaces *via* the same process as that used for GO. The UV-vis spectra and uranium adsorption capacities were measured to evaluate the functionalization and uranium adsorption efficiency of the samples, respectively. As shown in Fig. 6a, the peaks at 257 and 304 nm (the characteristic absorption of salicylaldoxime) appeared for all the oxime/PDA-modified substrates (solid lines). However, these two peaks were absent for all the substrates before modification (dashed lines).

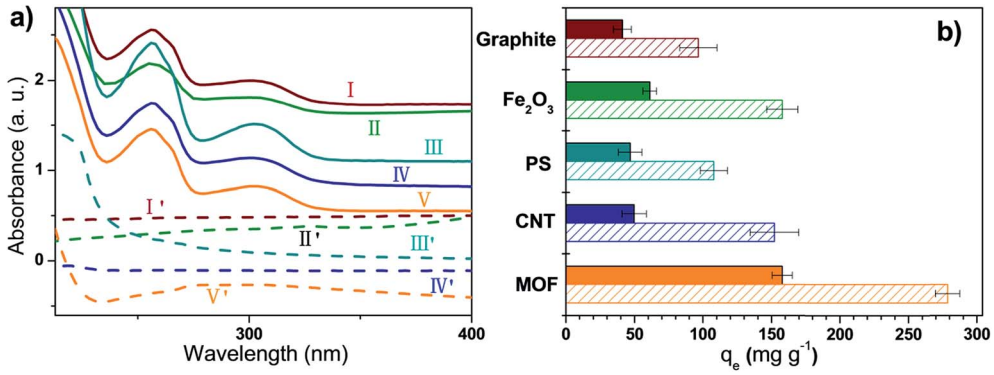

Fig. 6 (a) UV-vis spectra of oxime/PDA-modified graphite (I), Fe_2O_3 NPs (II), PS (III), CNTs (IV) and MOFs (V) prepared by this reported one-step process, respectively. The dashed lines (from I' to V') were the UV-vis spectra of the corresponding particles before oxime/PDA functionalization. (b) Uranium adsorption capacities of the graphite, Fe_2O_3 NPs, PS, CNTs and MOFs before (solid bars) and after (hatched bars) oxime/PDA modification. $C_o = 8$ mg L^{-1}, pH = 5.0 ± 0.1 and $T = 298$ K.

These results demonstrated that the oxime/PDA functionalized samples were prepared successfully. As shown in Fig. 6b, the adsorption amounts for the graphite, Fe_2O_3 NPs, PS, CNTs and MOFs (before oxime functionalization) were only 41.23, 61.13, 46.91, 49.76 and 157.80 mg g^{-1}, respectively. The adsorption amounts for the oxime/PDA modified substrates were 96.67, 157.80, 108.04, 152.11 and 278.73 mg g^{-1}, respectively, which were much larger than those for the bare substrates. These results indicated that improved adsorption capacities were obtained for these model substrates after oxime functionalization *via* this reported one-step process.

4 Conclusions

In this study, RGO-PDA/oxime was synthesized *via* a rapid one-step process based on the polymerization of DA and simultaneous deposition of salicylaldoxime. The maximum adsorption amount of uranium for the prepared RGO-PDA/oxime was 1049 mg g^{-1}, but the corresponding value for the RGO-PDA was only 675 mg g^{-1} originating from the introduced oxime groups on the surface of RGO-PDA/oxime. Meanwhile, this maximum adsorption amount was 3–16 times larger than those of the reported single PDA or oxime modified nanostructures, and the fabrication time (2 h) was only 1–19% of those of the reported oxime functionalized materials. Furthermore, this reported absorbent presented excellent selectivity (co-existing ions with high concentrations had a slight influence on the uranium sorption) and regeneration ability (the absorbent remained stable after four cycles of adsorption–desorption). Meanwhile, it was the homogeneous monolayer chemisorption, and the adsorption process agreed well with the second-order kinetics equation and Langmuir isotherm model. Finally, this one-step process was used to synthesize other oxime/PDA modified nanostructured materials, and the prepared samples exhibited an improved uranium adsorption capability. In conclusion, this developed method has great potential for use in the fabrication of uranium adsorbents on various surfaces, which can greatly contribute to resource sustainability and environmental safety.

Conflicts of interest

There are no conflicts to declare.

Acknowledgements

The financial support of the Finance Science and Technology Project of Hainan Province (No. DYF2018004), the National Natural Science Foundation of China (No. 51775152, 61761016 and 21574031), and the Start-up Scientific Research Foundation of Hainan University (No. KYQD(ZR)1818) is acknowledged.

Notes and references

1 A. Tolón-Becerra, X. Lastra-Bravo and F. Bienvenido-Bárcena, *Renewable Energy*, 2011, **36**, 2067–2077.
2 F. Wu, P. Ning, G. Ye, T. Sun, Z. Wang, S. Yang, W. Wang, X. Huo, Y. Lu and J. Chen, *Environ. Sci. Technol.*, 2017, **51**, 4606–4614.
3 (*a*) P. Yang, Q. Liu, J. Liu, H. Zhang, Z. Li, R. Li, L. Liu and J. Wang, *J. Mater. Chem. A*, 2017, **5**, 17933–17942; (*b*) X. Xiang, F. Pan and Y. Li, *Eng. Sci.*, 2018, **3**, 77–83, DOI: 10.30919/es8d736; (*c*) M. C. Kimling, N. Scales, T. L. Hanley and R. A. Caruso, *Environ. Sci. Technol.*, 2012, **46**, 7913–7920; (*d*) A. Zhang, X. Yin, X. Shen and Y. Liu, *ES Energy & Environment*, 2018, **1**, 89–98.
4 A. J. C. Semião, H. M. A. Rossiter and A. I. Schäfer, *J. Membr. Sci.*, 2010, **348**, 174–180.
5 K. W. Kim, J. T. Hyun, K. Y. Lee, E. H. Lee, K. W. Lee, K. C. Song and J. K. Moon, *J. Hazard. Mater.*, 2011, **193**, 52–58.
6 (*a*) M. J. Manos and M. G. Kanatzidis, *J. Am. Chem. Soc.*, 2012, **134**, 16441–16446; (*b*) M. L. Feng, D. Sarma, X. Qi, K. Z. Du, X. Y. Huang and M. G. Kanatzidis, *J. Am. Chem. Soc.*, 2016, **138**, 12578–12585.
7 F. Zaoui and M. A. Didi, *J. Radioanal. Nucl. Chem.*, 2013, **295**, 419–424.
8 (*a*) G. Yu, Y. Lu, J. Guo, M. Patel, A. Bafana, X. Wang, B. Qiu, C. Jeffryes, S. Wei and Z. Guo, *Adv. Compos. Hybrd. Mater.*,

2018, **1**, 56–78; (*b*) K. Gong, Q. Hu, L. Yao, M. Li, D. Sun, Q. Shao, B. Qiu and Z. Guo, *ACS Sustainable Chem. Eng.*, 2018, **6**, 7283–7291; (*c*) J. Huang, Y. Cao, Q. Shao, X. Peng and Z. Guo, *Ind. Eng. Chem. Res.*, 2017, **56**, 10689–10701; (*d*) H. Kang, Z. Cheng, H. Lai, H. Ma, Y. Liu, X. Mai, Y. Wang, Q. Shao, L. Xiang, X. Guo and Z. Guo, *Sep. Purif. Technol.*, 2018, **201**, 193–204; (*e*) Z. Yang, X. Hao, S. Chen, Z. Ma, W. Wang, C. Wang, L. Yue, H. Sun, Q. Shao, V. Murugadoss and Z. Guo, *J. Colloid Interface Sci.*, 2019, **533**, 13–23; (*f*) P. Zhang, T. Ge, H. Yang, S. Lin, Y. Cao, C. Zhao, H. Liu, A. Umar and Z. Guo, *Sci. Adv. Mater.*, 2018, **10**, 1216–1223; (*g*) J. Huang, Y. Li, Y. Cao, F. Peng, Y. Cao, Q. Shao, H. Liu and Z. Guo, *J. Mater. Chem. A*, 2018, **6**, 13062–13074; (*h*) J. Zhao, S. Ge, D. Pan, Q. Shao, J. Lin, Z. Wang, Z. Hu, T. Wu and Z. Guo, *J. Colloid Interface Sci.*, 2018, **529**, 111–121; (*i*) B. Zhao, Q. Shao, L. Hao, L. Zhang, Z. Liu, B. Zhang, S. Ge and Z. Guo, *J. Colloid Interface Sci.*, 2017, **511**, 39–47; (*j*) T. Wu, Q. Shao, S. Ge, L. Bao and Q. Liu, *RSC Adv.*, 2016, **6**, 58020–58027.

9 (*a*) H. Gu, X. Xu, H. Zhang, C. Liang, H. Lou, C. Ma, Y. Li, Z. Guo and J. Gu, *Eng. Sci.*, 2018, **1**, 46–54, DOI: 10.30919/espub.es.180308; (*b*) Y. Li, T. Jing, G. Xu, J. Tian, M. Dong, Q. Shao, B. Wang, Z. Wang, Y. Zheng, C. Yang and Z. Guo, *Polymer*, 2018, **149**, 13–22; (*c*) Y. Ma, L. Lyu, Y. Guo, Y. Fu, Q. Shao, T. Wu, S. Guo, K. Sun, X. Guo, E. K. Wujcik and Z. Guo, *Polymer*, 2017, **128**, 12–23; (*d*) Y. Wang, P. Zhou, S. Luo, S. Guo, J. Lin, Q. Shao, X. Guo, Z. Liu, J. Shen, B. Wang and Z. Guo, *Adv. Polym. Technol.*, 2018, 1–16; (*e*) Y. Wang, P. Zhou, S. Luo, X. Liao, B. Wang, Q. Shao, X. Guo and Z. Guo, *Langmuir*, 2018, **34**, 7859–7868; (*f*) Z. Li, B. Wang, X. Qin, Y. Wang, C. Liu, Q. Shao, N. Wang, J. Zhang, Z. Wang, C. Shen and Z. Guo, *ACS Sustainable Chem. Eng.*, 2018, **6**, 13747–13755; (*g*) H. Zhang, S. Lyu, X. Zhou, H. Gu, C. Ma, C. Wang, T. Ding, Q. Shao, H. Liu and Z. Guo, *J. Colloid Interface Sci.*, 2019, DOI: 10.1016/j.jcis.2018.10.038; (*h*) K. Gong, Q. Hu, Y. Xiao, X. Cheng, H. Liu, N. Wang, B. Qiu and Z. Guo, *J. Mater. Chem. A*, 2018, **6**, 11119–11128; (*i*) K. Gong, S. Guo, Y. Zhao, Q. Hu, H. Liu, D. Sun, M. Li, B. Qiu and Z. Guo, *J. Mater. Chem. A*, 2018, **6**, 16824–16832.

10 L. L. Wang, F. Luo, L. L. Dang, J. Q. Li, X. L. Wu, S. J. Liu and M. B. Luo, *J. Mater. Chem. A*, 2015, **3**, 13724–13730.

11 S. Yang, J. Qian, L. Kuang and D. Hua, *ACS Appl. Mater. Interfaces*, 2017, **9**, 29337–29344.

12 J. Górka, R. T. Mayes, L. Baggetto, G. M. Veith and S. Dai, *J. Mater. Chem. A*, 2013, **1**, 3016–3026.

13 (*a*) D. Shao, G. Hou, J. Li, W. Tao, X. Ren and X. Wang, *Chem. Eng. J.*, 2014, **255**, 604–612; (*b*) Z. Wang, H. Zhu, N. Cao, R. Du, Y. Liu and G. Zhao, *Mater. Lett.*, 2017, **186**, 274–278; (*c*) Z. Zhao, R. Guan, J. Zhang, Z. Zhao and P. Bai, *Acta Metall. Sin. (Engl. Lett.)*, 2017, **30**, 66–72; (*d*) Z. Zhao, P. Bai1, R. Guan, V. Murugadoss, H. Liu, X. Wang and Z. Guo, *Mater. Sci. Eng., A*, 2018, **734**, 200–209; (*e*) Y. Zhao, S. Deng, H. Liu, J. Zhang, Z. Guo and H. Hou, *Comput. Mater. Sci.*, 2018, **154**, 365–370; (*f*) C. Wang, Z. He, X. Xie, X. Mai, Y. Li, T. Li, M. Zhao, C. Yan, H. Liu, E. Wujcik and Z. Guo, *Macromol. Mater. Eng.*, 2018, **3**, 1700462; (*g*) H. Du, C. Zhao, J. Lin, Z. Hu, Q. Shao, J. Guo, B. Wang, D. Pan, E. K. Wujcik and Z. Guo, *Chem. Rec.*, 2018, **18**, 1365–1372; (*h*) M. Dong, Q. Li, H. Liu, C. Liu, E. Wujcik, Q. Shao, T. Ding, X. Mai, C. Shen and Z. Guo, *Polymer*, 2018, **158**, 381–390; (*i*) W. Du, X. Wang, J. Zhan, X. Sun, L. Kang, F. Jiang, X. Zhang, Q. Shao, M. Dong, H. Liu, V. Murugadoss and Z. Guo, *Electrochim. Acta*, 2018, DOI: 10.1016/j.electacta.2018.11.074.

14 (*a*) C. W. Abney, R. T. Mayes, T. Saito and S. Dai, *Chem. Rev.*, 2017, **117**, 13935–14013; (*b*) C. Wang, B. Mo, Z. He, Q. Shao, D. Pan, E. Wujick, J. Guo, X. Xie, X. Xie and Z. Guo, *J. Membr. Sci.*, 2018, **556**, 118–125; (*c*) C. Wang, B. Mo, Z. He, C. X. Zhao, L. Zhang, Q. Shao, X. Guo, E. Wujcik and Z. Guo, *Polymer*, 2018, **138**, 363–368; (*d*) C. Wang, V. Murugadoss, J. Kong, Z. He, X. Mai, Q. Shao, Y. Chen, L. Guo, C. Liu, S. Angaiah and Z. Guo, *Carbon*, 2018, **140**, 696–733; (*e*) D. Jiang, V. Murugadoss, Y. Wang, J. Lin, T. Ding, Z. Wang, Q. Shao, C. Wang, H. Liu, N. Lu, R. Wei, S. Angaiah and Z. Guo, *Polym. Rev.*, 2018, DOI: 10.1080/15583724.2018.1546737; (*f*) Z. Zhao, H. An, J. Lin, M. Feng, V. Murugadoss, T. Ding, H. Liu, Q. Shao, X. Man, N. Wang, H. Gu, S. Angaiah and Z. Guo, *Chem. Rec.*, 2019, DOI: 10.1002/tcr.201800153; (*g*) N. Wu, C. Liu, D. Xu, J. Liu, W. Liu, Q. Shao and Z. Guo, *ACS Sustainable Chem. Eng.*, 2018, **6**, 12471–12480; (*h*) H. Liu, Q. Li, S. Zhang, R. Yin, X. Liu, Y. He, K. Dai, C. Shan, J. Guo, C. Liu, C. Shen, X. Wang, N. Wang, Z. Wang, R. Wei and Z. Guo, *J. Mater. Chem. C*, 2018, **6**, 12121–12141; (*i*) H. Wei, H. Wang, Y. Xia, D. Cui, Y. Shi, M. Dong, C. Liu, T. Ding, J. Zhang, Y. Ma, N. Wang, Z. Wang, Y. Sun, R. Wei and Z. Guo, *J. Mater. Chem. C*, 2018, DOI: 10.1039/c8tc04515a; (*j*) Z. Li, B. Wang, X. Qin, Y. Wang, C. Liu, Q. Shao, N. Wang, J. Zhang, Z. Wang, C. Shen and Z. Guo, *ACS Sustainable Chem. Eng.*, 2018, **6**, 13747–13755; (*k*) Y. Zhao, L. Qi, Y. Jin, K. Wang, J. Tian and P. Han, *J. Alloys Compd.*, 2015, **647**, 1104–1110.

15 S. Vukovic, L. A. Watson, S. O. Kang, R. Custelcean and B. P. Hay, *Inorg. Chem.*, 2012, **51**, 3855–3859.

16 L. Chen, Z. Bai, L. Zhu, L. Zhang, Y. Cai, Y. Li, W. Liu, Y. Wang, L. Chen and J. Diwu, *ACS Appl. Mater. Interfaces*, 2017, **9**, 32446–32451.

17 S. Brown, S. Chatterjee, M. Li, Y. Yue, C. Tsouris, C. J. Janke, T. Saito and S. Dai, *Ind. Eng. Chem. Res.*, 2016, **55**, 4130–4138.

18 X. Lu, D. Zhang, A. T. Reda, C. Liu, Z. Yang, S. Guo, S. Xiao and Y. Ouyang, *Ind. Eng. Chem. Res.*, 2017, **56**, 11936–11947.

19 Y. Zhao, J. Li, L. Zhao, S. Zhang, Y. Huang, X. Wu and X. Wang, *Chem. Eng. J.*, 2014, **235**, 275–283.

20 Y. Oyola, C. J. Janke and S. Dai, *Ind. Eng. Chem. Res.*, 2016, **55**, 4149–4160.

21 G. Tian, S. J. Teat, Z. Zhang and L. Rao, *Dalton Trans.*, 2012, **41**, 11579–11586.

22 Q. Sun, B. Aguila, J. Perman, A. S. Ivanov, V. S. Bryantsev, L. D. Earl, C. W. Abney, L. Wojtas and S. Ma, *Nat. Commun.*, 2018, **9**, 1644.

23 H. Lee, S. M. Dellatore, W. M. Miller and P. B. Messersmith, *Science*, 2007, **318**, 426–430.

24 R. A. Zangmeister, T. A. Morris and M. J. Tarlov, *Langmuir*, 2013, **29**, 8619–8628.

25 Y. He, J. Wang, H. Zhang, T. Zhang, B. Zhang, S. Cao and J. Liu, *J. Mater. Chem. A*, 2014, **2**, 9548–9558.
26 Y. Liu, K. Ai and L. Lu, *Chem. Rev.*, 2014, **114**, 5057–5115.
27 O. Pop-Georgievski, D. Verreault, M. O. Diesner, V. Proks, S. Heissler, F. Rypáček and P. Koelsch, *Langmuir*, 2012, **28**, 14273–14283.
28 N. F. D. Vecchia, R. Avolio, M. Alfè, M. E. Errico, A. Napolitano and M. D'Ischia, *Adv. Funct. Mater.*, 2013, **23**, 1331–1340.
29 Q. Ye, F. Zhou and W. Liu, *Chem. Soc. Rev.*, 2011, **40**, 4244–4258.
30 J. Park, T. F. Brust, J. L. Hong, C. L. Sang, V. J. Watts and Y. Yeo, *ACS Nano*, 2014, **8**, 3347–3356.
31 L. Bai, S. Duan, W. Jiang, M. Liu, S. Wang, M. Sang, X. Gong, J. Li and S. Xuan, *Appl. Surf. Sci.*, 2017, **426**, 1121–1132.
32 G. Jun-Kai, H. Li-An, Z. Guang-Hui and G. Ping, *J. Hazard. Mater.*, 2015, **286**, 325–333.
33 S. H. Hwang, D. Kang, R. S. Ruoff, H. S. Shin and Y. B. Park, *ACS Nano*, 2014, **8**, 6739–6747.
34 S. M. Kang, S. Park, D. Kim, S. Y. Park, R. S. Ruoff and H. Lee, *Adv. Funct. Mater.*, 2011, **21**, 108–112.
35 H. Bai, C. Li, X. Wang and G. Shi, *J. Phys. Chem. C*, 2011, **115**, 5545–5551.
36 G. Wang, X. Wang, X. Chai, J. Liu and N. Deng, *Appl. Clay Sci.*, 2010, **47**, 448–451.
37 J. Li, Z. Guo, S. Zhang and X. Wang, *Chem. Eng. J.*, 2011, **172**, 892–897.
38 G. Tian, J. Geng, Y. Jin, C. Wang, S. Li, Z. Chen, H. Wang, Y. Zhao and S. Li, *J. Hazard. Mater.*, 2011, **190**, 442–450.
39 Y. Wang, Z. Gu, J. Yang, J. Liao, Y. Yang, N. Liu and J. Tang, *Appl. Surf. Sci.*, 2014, **320**, 10–20.
40 B. Li, Q. Sun, Y. Zhang, C. W. Abney, B. Aguila, W. Lin and S. Ma, *ACS Appl. Mater. Interfaces*, 2017, **9**, 12511–12517.
41 Z. Li, F. Chen, L. Yuan, Y. Liu, Y. Zhao, Z. Chai and W. Shi, *Chem. Eng. J.*, 2012, **210**, 539–546.
42 Y. R. He, S. C. Li, X. L. Li, Y. Yang, A. N. Tang, L. Du, Z. Y. Tan, D. Zhang and H. B. Chen, *Chem. Eng. J.*, 2018, **338**, 333–340.
43 L. Tan, Y. Wang, Q. Liu, J. Wang, X. Jing, L. Liu, J. Liu and D. Song, *Chem. Eng. J.*, 2015, **259**, 752–760.
44 C. Gunathilake, J. Gorka, S. Dai and M. Jaroniec, *J. Mater. Chem. A*, 2015, **3**, 11650–11659.
45 K. Tian, J. Wu and J. Wang, *Radiochim. Acta*, 2018, **106**, 719–731.
46 C. C. Ding, W. C. Cheng, X. Q. Nie and F. C. Yi, *Chem. Eng. J.*, 2017, **324**, 113–121.
47 H. B. Pan, W. Liao, C. M. Wai, Y. Oyola, C. J. Janke, G. Tian and L. Rao, *Dalton Trans.*, 2014, **43**, 10713–10718.